Departmental Papers (ESE)   Department of Electrical & Systems Engineering

January 1990

The Theory of Chirowaveguides

Philippe Pelet
University of Pennsylvania

Nader Engheta
University of Pennsylvania, engheta@ee.upenn.edu

The Theory of Chirowaveguides

Abstract

Recently a new type of guided-wave structure, named *chirowaveguide* was suggested by the authors. The chirowaveguides consist of cylindrical waveguides filled with homogeneous isotropic chiral materials. Due to the *electromagnetic chirality* of the material inside the waveguide, several important features area associated with this type of guided-wave structure. In this paper, the theory of chirowaveguides is discussed and their salient features are analyzed. It is show that the Helmhotz equations for the longitudinal components of electric and magnetic fields in chirowaveguides are always coupled and consequently, in these waveguides individual transverse electric (TE), transverse magnetic (TM), or transverse electromagnetic (TEM) modes cannot be supported. As an illustrative example, the parallel-plate chirowaveguide is analyzed in detail and the corresponding dispersion relations, cut-off frequencies, propagating and evanescent modes are obtained. In the dispersion (Brillouin) diagram for a chirowaveguide, three regions are identified: the *fast-fast-wave* region, the *fast-slow-wave* region and the *slow-slow-wave* region. For each of these regions the electromagnetic field components in a parallel-plat chirowaveguide are analyzed and the electric field components are plotted. Potential applications of chirowaveguides in integrated optical devices, communication systems, and printed circuit antennas are mentioned.

Comments

The Theory of Chirowaveguides

PHILIPPE PELET, STUDENT MEMBER, IEEE, AND NADER ENGHETA, SENIOR MEMBER, IEEE

Abstract—Recently a new type of guided-wave structure, named *chirowaveguide* was suggested by the authors. The chirowaveguides consist of cylindrical waveguides filled with homogeneous isotropic chiral materials. Due to the *electromagnetic chirality* of the material inside the waveguide, several important features are associated with this type of guided-wave structure. In this paper, the theory of chirowaveguides is discussed and their salient features are analyzed. It is shown that the Helmholtz equations for the longitudinal components of electric and magnetic fields in chirowaveguides are always coupled and consequently, in these waveguides individual transverse electric (TE), transverse magnetic (TM), or transverse electromagnetic (TEM) modes cannot be supported. As an illustrative example, the parallel-plate chirowaveguide is analyzed in detail and the corresponding dispersion relations, cut-off frequencies, propagating and evanescent modes are obtained. In the dispersion (Brillouin) diagram for a chirowaveguide, three regions are identified: the *fast-fast-wave* region, the *fast-slow-wave* region and the *slow-slow-wave* region. For each of these regions the electromagnetic field components in a parallel-plate chirowaveguide are analyzed and the electric field components are plotted. Potential applications of chirowaveguides in integrated optical devices, communication systems, and printed circuit antennas are mentioned.

I. INTRODUCTION

THE CONCEPT OF *electromagnetic chirality* embraces both optical activity and circular dichroism[1] [1], [2]. The phenomenon of optical activity was discovered by Arago in 1811 [3]. He found that crystals of quartz rotate the plane of polarization of linearly polarized light transmitted in the direction of its optical axis. Shortly thereafter, experimentation by Biot [4]–[6] on plates of quartz put in evidence the dependence of optical activity on the thickness of the plates of crystal and on the light wavelength. Furthermore, he discovered that the optical activity also appears in certain liquids. In 1848, Pasteur [7] postulated that molecules of optically active materials are three-dimensional *chiral* figures, and the *chirality* or handedness of these molecules causes optical activity. In other words, optical activity is a manifestation of the chirality of these molecules.

Chirality or handedness is a purely geometric notion that refers to the lack of bilateral symmetry of an object. A three-dimensional chiral object is, by definition, a body that cannot be brought into congruence with its mirror image by translation and rotation [8], [9]. Such a body has the property of handedness and is either right-handed or left-handed. Many of

[1] Optical activity refers to the rotation of the plane of polarization of optical waves by a medium while circular dichroism indicates a change in the polarization ellipticity of optical waves by a medium.

naturally occurring and man-made objects fall into the category of chiral objects. A variety of sugar arrays, amino acids, DNA and organic polymers are among the natural chiral objects while such common objects as wire helices, the Möbius strip and the irregular tetrahedron are considered the man-made chiral objects.

It has been shown that in the case of a chiral medium made of randomly oriented and uniformly distributed lossless, short, wire helices, the set of constitutive relations for time-harmonic fields ($e^{-i\omega t}$) has the form

$$D = \epsilon E + i\xi_c B \tag{1}$$

$$H = i\xi_c E + B/\mu \tag{2}$$

where ϵ, μ, ξ_c are real constants and represent the dielectric constant, permeability, and chirality admittance of the chiral medium, respectively. Moreover, it has been conjectured that (1) and (2) apply not only to chiral media composed of helices but also to any lossless, reciprocal, chiral media composed of chiral objects of arbitrary shape [10]. The fundamentals of chiral constitutive relations have been treated in books by Kong [11] and Post [12]. Chirality and its effects in optical activity began to attract attention in the electromagnetics community with the microwave experiments of Lindman [13], [14] and Pickering [15]. In the microwave regime, they obtained results somewhat similar to those for the optical frequencies. They devised a macroscopic model for the phenomenon by using microwave instead of light, and wire helices instead of chiral molecules. They illustrated the molecular process responsible for optical activity using this model. In the most recent past, the following papers are among those on wave interaction with chiral media: the work on transition radiation at a dielectric-chiral interface [16], electromagnetic wave propagation through a chiral slab [17], the electromagnetic properties of bianisotropic media [18], [11], [12], the reflection of waves from achiral-chiral interfaces [17], [19], [20], the dyadic Green's functions and dipole radiation in an unbounded, isotropic, lossless chiral medium [21], [22] and the canonical sources and duality in chiral media [23].

In this paper, we study and analyze electromagnetic wave propagation in guided-wave structures containing chiral materials. Such guided-wave structures we named *chirowaveguides* [1]. The motivation for this study, besides its theoretical and academic importance, is provided by potential applications of chiral materials to integrated optical devices, optical waveguides and printed-circuit elements. Furthermore, with recent advances in polymer science, it is believed that chiral materials for the millimeter wave and microwave regimes can be made. This will open a new chapter in the design of
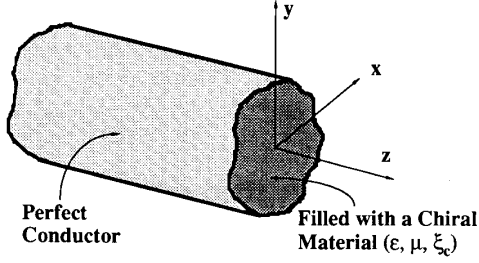
Fig. 1. A cylindrical chirowaveguide which consists of a cylindrical waveguide filled with a homogeneous lossless isotropic chiral material (ϵ, μ, ξ_c). The axis of the cylinder, which is the direction of propagation of guided waves, is denoted by z axis.

millimeter-wave components and devices. Here, the general features of chirowaveguides are studied, and as an example, the case of a parallel-plate waveguide filled with a chiral material is investigated in detail.

II. FORMULATION OF THE PROBLEM

Consider a cylindrical waveguide of arbitrary cross section with its axis in the direction of the z axis and filled with a homogeneous, lossless, isotropic chiral material described by (1) and (2). The boundary surfaces will be assumed to be perfect conductor (Fig. 1). The propagation is in the z direction and, therefore, all the electromagnetic field components have $e^{\gamma z}$ as the z dependence, where γ is, in general, a complex quantity.

From the chiral constitutive relations (1) and (2), and the source-free Maxwell equations, we find

$$\nabla \times \nabla \times \begin{Bmatrix} \mathbf{E} \\ \mathbf{H} \end{Bmatrix} - 2\omega\mu\xi_c \nabla \times \begin{Bmatrix} \mathbf{E} \\ \mathbf{H} \end{Bmatrix} - k^2 \begin{Bmatrix} \mathbf{E} \\ \mathbf{H} \end{Bmatrix} = 0, \quad (3)$$

where $k = \omega\sqrt{\mu\epsilon}$ with ω being the radian frequency of the time-harmonic fields [21], [22]. It is known that, for a plane wave propagation in an unbounded chiral medium, there exist two bulk eigenmodes of propagation, a right circularly polarized (RCP) and a left circularly polarized (LCP) plane wave with wavenumbers

$$k_\pm = \pm\omega\mu\xi_c + \sqrt{k^2 + (\omega\mu\xi_c)^2}. \quad (4)$$

In the waveguide under study, however, the wavenumber along the z axis is γ to be determined for given frequencies. Considering the z dependence $e^{\gamma z}$ for the field components inside the guide and using chiral constitutive relations (1) and (2) and the source-free Maxwell equations, the transverse components of electric and magnetic fields inside the chirowaveguide can be expressed in terms of the longitudinal components of $\mathbf{E}$ and $\mathbf{H}$. These relations can be written in the following compact form:

$$[E_x; E_y; H_x; H_y]^T = \frac{[a_{ij}]}{h^2} \left[\frac{\partial E_z}{\partial x}; \frac{\partial E_z}{\partial y}; \frac{\partial H_z}{\partial x}; \frac{\partial H_z}{\partial y}\right]^T$$

$$(5)$$

where

$$\begin{cases} a_{11} = a_{22} = a_{33} = a_{44} = \gamma \left[\gamma^2 + \frac{k_+^2 + k_-^2}{2}\right] \\ a_{12} = -a_{21} = a_{34} = -a_{43} = -\omega\mu\xi_c \left[k^2 - \gamma^2\right] \\ a_{13} = a_{24} = -2i\omega^2\mu^2\gamma\xi_c \\ a_{14} = -a_{23} = i\omega\mu \left[k^2 + \gamma^2\right] \\ a_{31} = a_{42} = 2i\omega^2\mu^2\gamma\xi_c/\eta_c^2 \\ a_{32} = -a_{41} = -i\omega\mu \left[k^2 + \gamma^2\right]/\eta_c^2 \end{cases}$$

and $h^2 = (\gamma^2 + k_+^2)(\gamma^2 + k_-^2)$, $\eta = \sqrt{\mu/\epsilon}$, $\eta_c^2 = \eta^2/(1 + \eta^2\xi_c^2)$ and $[\ ]^T$ denotes the transpose of a matrix. These relations are generalization of a nonchiral case where $\xi_c = 0$. From (5) and the wave equations (3), we obtain the following set of equations for the z components of the field vectors $\mathbf{E}$ and $\mathbf{H}$:

$$\left[\frac{\partial^2}{\partial x^2} + \frac{\partial^2}{\partial y^2}\right] \begin{Bmatrix} E_z \\ H_z \end{Bmatrix} + \left[\gamma^2 + \frac{k_+^2 + k_-^2}{2}\right] \begin{Bmatrix} E_z \\ H_z \end{Bmatrix}$$

$$\pm 2i\omega^2\mu^2\xi_c \begin{Bmatrix} H_z \\ (1/\eta_c^2)E_z \end{Bmatrix} = 0. \quad (6)$$

The above equations are *coupled* equations for the longitudinal components of the fields $\mathbf{E}$ and $\mathbf{H}$. The boundary conditions needed for solving (6) are obtained by equating to zero the tangential components of $\mathbf{E}$ on the surface of the chirowaveguide. Having obtained E_z and H_z from (6) and the proper boundary conditions, one can find the transverse components of $\mathbf{E}$ and $\mathbf{H}$ from (5). We observe that for conventional waveguides filled with nonchiral media, i.e., for $\xi_c = 0$, (6) reduces to a set of *decoupled* Helmholtz equations for longitudinal field components.

From (6), we note that it is impossible for E_z or H_z to be identically zero unless they are both zero. In other words, neither TM nor TE modes can exist individually in a chirowaveguide. When E_z and H_z are both zero, from (5) we observe that either all the transverse components are zero or $h = 0$. If all the transverse components are zero, the fields will vanish identically. If $h = 0$, one can show, from Maxwell's equations, that $\nabla_t \times \mathbf{E}_t = 0$ and $\mathbf{E}_t = \pm i\mathbf{e}_z \times \mathbf{E}_t$ where $\mathbf{e}_z$ is the unit vector along the z axis, $\nabla_t = \nabla - (\partial/\partial z)\mathbf{e}_z$ and the subscript t denotes the projection of a vector on the xy plane transverse to the direction of propagation. The first relation implies that $\mathbf{E}_t$ can be chosen to be $\mathbf{E}_t = \nabla_t\Psi$ where Ψ is an arbitrary function of x and y. Using the second relation, the scalar function Ψ is proved to be an analytic function. Since the tangential component of $\mathbf{E}_t$ must vanish on the boundary, Ψ must be constant over this boundary, and therefore it follows from the theory of analytic functions that Ψ is constant over the entire cross section of the waveguide. This implies that $\mathbf{E}_t = 0$ everywhere on the transverse plane. Hence, propagating modes in chirowaveguides are all hybrid and *individual* transverse electric (TE), transverse magnetic (TM) or transverse electromagnetic (TEM) *modes cannot be supported in a chirowaveguide*. Cylindrical waveguides filled with magnetically biased ferrites present somewhat similar character-
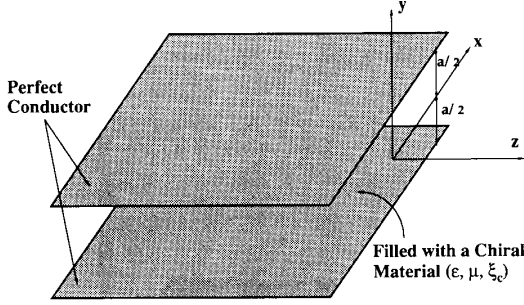
Fig. 2. A parallel-plate chirowaveguide. In this chirowaveguides, the direction of propagation is along z axis. The field quantities are all independent of x axis.

istics [24]-[28]. However, it should be noted that chirowaveguides, due to the reciprocal nature of chiral materials, are reciprocal elements while waveguides containing magnetized ferrites are not.

Returning to the set of equations in (6), let us attempt to transform them to a pair of decoupled equations by expressing E_z and H_z in terms of two new functions U_1 and U_2 as follows:

$$\begin{cases} E_z = p_1 U_1 + p_2 U_2 \\ H_z = q_1 U_1 + q_2 U_2 \end{cases} \tag{7}$$

where p_1, p_2, q_1 and q_2 are constants to be chosen. In order not to lose generality, we also assume that $p_1 q_2 - p_2 q_1 \neq 0$. Substituting (7) into (6), we obtain

$$\begin{cases} \nabla_t^2 U_1 + S_1 U_1 = 0 \\ \nabla_t^2 U_2 + S_2 U_2 = 0 \end{cases} \tag{8}$$

where $S_1 = k_+^2 + \gamma^2$, $S_2 = k_-^2 + \gamma^2$, and the constants p_1, p_2, q_1 and q_2 have been found to be $p_1 = S_1$, $p_2 = S_2$, $q_1 = (k_+^2 - k_-^2)S_1/(4i\omega^2\mu^2\xi_c)$ and $q_2 = -(k_+^2 - k_-^2)S_2/(4i\omega^2\mu^2\xi_c)$. One can now find the solutions U_1 and U_2 of the equations (8) subject to the boundary conditions for the field quantities **E** and **H**. Then, the longitudinal and transverse field components can be obtained from (7) and (5).

III. PARALLEL-PLATE CHIROWAVEGUIDES AND THEIR IMPORTANT FEATURES

Up to this point the cross section of the waveguide has been assumed to be arbitrary. Now as an illustrative example, let us consider a parallel-plate chirowaveguide (Fig. 2). This waveguide consists of two parallel perfectly conducting planes of infinite extent in the x and z directions, and is filled with a lossless, homogeneous, isotropic chiral material described by (1) and (2). Without loss of generality, it is assumed that the chirality admittance ξ_c is a positive quantity. However, it should be noted that the analysis described hereafter is also valid for negative values of ξ_c as long as the roles of k_+ and k_-, as well as RCP and LCP waves, are interchanged. The separation of the two plates is taken to be a. For propagating modes in the z direction, the propagation constant γ must be an imaginary quantity. Thus γ can be written as $\gamma = i\beta$ where

β is a real quantity to be determined. The field quantities are assumed to be independent of the x coordinate.

Following the approach described in the previous section, we find the solutions to (8). They are

$$U_1 = A_{11} \cos(\sqrt{S_1}\, y) + A_{12} \sin(\sqrt{S_1}\, y) \tag{9a}$$

$$U_2 = A_{21} \cos(\sqrt{S_2}\, y) + A_{22} \sin(\sqrt{S_2}\, y) \tag{9b}$$

where A_{11}, A_{12}, A_{21}, and A_{22} are constants to be determined and S_1 and S_2 are defined earlier. Imposing the boundary conditions for the field quantities, we obtain a set of homogeneous algebraic equations for these constants. For a nontrivial solution of this, the determinant of coefficients must be zero. This leads to the following equation for propagating modes for $\gamma = i\beta$

$$2\sqrt{[1 - (\beta/k_+)^2][1 - (\beta/k_-)^2]}$$
$$\cdot \{1 - \cos(k_+ a\sqrt{1 - (\beta/k_+)^2}) \cos(k_- a\sqrt{1 - (\beta/k_-)^2})\}$$
$$+ \{2 - (\beta/k_+)^2 - (\beta/k_-)^2\} \sin(k_+ a\sqrt{1 - (\beta/k_+)^2})$$
$$\cdot \sin(k_- a\sqrt{1 - (\beta/k_-)^2}) = 0. \tag{10}$$

This is the dispersion relation for propagating modes in a parallel-plate lossless chirowaveguide.

It is well known that in conventional rectangular waveguides filled with homogeneous nonchiral materials, field configuration can be obtained by superposing two or more plane waves in a suitable manner. These plane waves propagate with the unbounded-medium or bulk wavenumber. In a conventional parallel-plate waveguide, this separation into component waves is quite simple. In those waveguides, there are only two component waves, and the direction of these waves depends upon the frequency and the dimension a. In a parallel-plate chirowaveguide, however, due to the fact that chiral media support double-mode propagation (k_+ and k_-), there are four component waves. Two of the waves are RCP propagating with wavenumber k_+, and the other two are LCP propagating with wavenumber k_-. Fig. 3 shows these waves in a parallel-plate chirowaveguide. Consider R_1, R_2, L_1 and L_2 to be the amplitudes of the component waves E_{R1}, E_{R2}, E_{L1} and E_{L2}, respectively. Thus, these waves can be expressed as follows:

$$\mathbf{E}_{R1} = R_1 e^{ik_+ \cdot (z \cos\theta + y \sin\theta)}\mathbf{e}_{R1},$$

$$\mathbf{E}_{R2} = R_2 e^{ik_+ \cdot (z \cos\theta - y \sin\theta)}\mathbf{e}_{R2},$$

$$\mathbf{E}_{L1} = L_1 e^{ik_- \cdot (z \cos\varphi + y \sin\varphi)}\mathbf{e}_{L1},$$

$$\mathbf{E}_{L2} = L_2 e^{ik_- \cdot (z \cos\varphi - y \sin\varphi)}\mathbf{e}_{L2} \tag{11}$$

where $\mathbf{e}_{R1}$, $\mathbf{e}_{R2}$, $\mathbf{e}_{L1}$ and $\mathbf{e}_{L2}$ are the circular basis unit vectors for the right and left circularly polarized waves in the directions θ and φ (Fig. 3). Since the guided wave propagates in the z direction with propagation constant β, the z component of the bulk mode wavenumbers must equal β. Hence

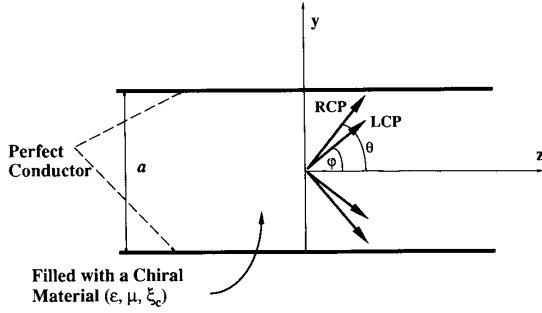$$k_+ \cos\theta = k_- \cos\varphi = \beta. \tag{12}$$

Fig. 3. Cross-sectional view of the parallel-plate chirowaveguide with four component (bulk) plane waves two of which are RCP propagating with wavenumber k_+ and the other two are LCP propagating with wavenumber k_-. The arrows indicate the directions of propagation of the four bulk plane waves.

Applying the boundary conditions at $y = -a/2$ and $y = a/2$, we obtain the following set of equations for coefficients R_1, R_2, L_1 and L_2

$$(R_1, R_2, L_1, L_2)[A]^T = 0 \tag{13}$$

where

$$[A]^T = \begin{pmatrix} e^{-ik_+a \sin \theta/2} & -i\sin\theta e^{-ik_+a \sin \theta/2} & e^{ik_+a \sin \theta/2} & -i\sin\theta e^{ik_+a \sin \theta/2} \\ e^{ik_+a \sin \theta/2} & i\sin\theta e^{ik_+a \sin \theta/2} & e^{-ik_+a \sin \theta/2} & i\sin\theta e^{-ik_+a \sin \theta/2} \\ e^{-ik_-a \sin \varphi/2} & i\sin\varphi e^{-ik_-a \sin \varphi/2} & e^{ik_-a \sin \varphi/2} & i\sin\varphi e^{ik_-a \sin \varphi/2} \\ e^{ik_-a \sin \varphi/2} & -i\sin\varphi e^{ik_-a \sin \varphi/2} & e^{-ik_-a \sin \varphi/2} & -i\sin\varphi e^{-ik_-a \sin \varphi/2} \end{pmatrix}. \tag{14}$$

Nontrivial solutions are obtained when $\det[A] = 0$. This leads to

$$2 \sin \theta \sin \varphi\{1 - \cos(k_+a \sin \theta) \cos(k_-a \sin \varphi)\}$$

$$+\{\sin \theta^2 + \sin \varphi^2\} \sin(k_+a \sin \theta) \sin(k_-a \sin \varphi) = 0, \tag{15}$$

which is equivalent to (10). This is another form of the dispersion relation in the parallel-plate chirowaveguide in terms of angles θ and φ. From this relation, one can obtain the dispersion relation (10) substituting $\theta = \cos^{-1}(\beta/k_+)$ and $\varphi = \cos^{-1}(\beta/k_-)$. The problem is, now, to solve (10) (or (15)) for any given frequency and to obtain the propagation constant β or angles θ and φ subject to the condition (12). Propagating modes have real β. However, when β is imaginary, i.e., $\beta = i\alpha$, we have evanescent modes. These two types of mode in the parallel-plate chirowaveguide will be discussed in the following subsections.

A. Propagating Modes

For modes propagating in the positive z direction, the propagation constant β is a real positive quantity. Since there exist two bulk wavenumbers k_+ and k_- for an unbounded chiral material, there are three regions in the dispersion or $\omega - \beta$ diagram for the propagation constant β, viz.

Region I: $\beta < k_- < k_+$, for $\xi_c > 0$ (16)

Region II: $k_- < \beta < k_+$, for $\xi_c > 0$ (17)

Region III: $k_- < k_+ < \beta$, for $\xi_c > 0$. (18)

In region I, the phase velocity of the guided wave, i.e., $v_{p,z} = \omega/\beta$ is greater than both velocities $v_+ = \omega/k_+$ and $v_- = \omega/k_-$. That is

$$v_{p,z} > v_- > v_+, \qquad \text{for } \xi_c > 0. \tag{19}$$

Therefore we refer to this region as the *fast-fast-wave* region. In region II, however, we have

$$v_- > v_{p,z} > v_+, \qquad \text{for } \xi_c > 0, \tag{20}$$

and hence we call it, the *fast-slow-wave* region. Finally, region III is named the *slow-slow-wave* region because

$$v_- > v_+ > v_{p,z} \qquad \text{for } \xi_c > 0. \tag{21}$$

Now we study each region of the dispersion diagram separately.

1) Fast-Fast-Wave Region: In this region of $\omega - \beta$ diagram where $\beta < k_- < k_+$ for $\xi_c > 0$, the angles θ and φ are real and have values between $0°$ and $90°$. The $\omega - \beta$ diagram, which is also called Brillouin diagram is presented in Fig. 4 for $\xi_c = 0.001$ mho. In this figure, the dimensionless quantity $\Omega \equiv \omega a \sqrt{\mu\epsilon}$ is plotted versus the dimensionless guide wavenumber along the z direction, i.e., $\beta a = k_+a \cos \theta$. The fast-fast-wave region is restricted to the region between the Ω axis and the line k_- in the $\omega - \beta$ diagram.

The cut-off frequencies are those at which the propagation constant $\beta = 0$, and consequently $\theta = \varphi = 90°$. From (10), we obtained the following expression for the cut-off frequencies in a parallel-plate chirowaveguide:

$$\Omega_c \equiv \omega_c a \sqrt{\mu\epsilon} = \frac{n\pi}{\sqrt{\frac{\mu}{\epsilon}\xi_c^2 + 1}} = n\pi\frac{\eta_c}{\eta} \tag{22}$$

where $n = 1, 2, 3 \cdots$ and η_c is already defined. These frequencies are shown as points A_1, A_2, $\cdots$ in Fig. 4. Equivalently, the cut-off wavelengths can be written as

$$\frac{a}{\lambda_c} = \frac{n}{2\sqrt{\frac{\mu}{\epsilon}\xi_c^2 + 1}} \tag{23}$$

where λ_c is the cut-off wavelength as measured in the medium with $\xi_c = 0$. Since $\eta_c/\eta < 1$, from (22) and Fig. 4, we note that the cut-off frequencies are closer to each other than those
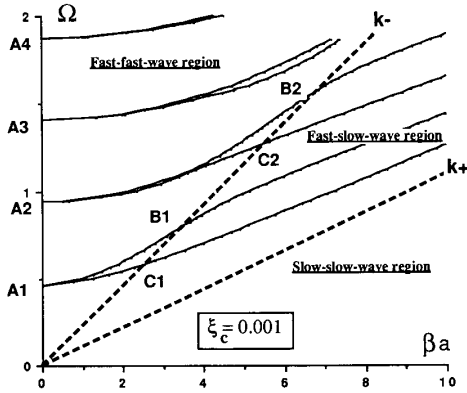
Fig. 4.   Dispersion (Brillouin) diagram for propagating modes in a parallel-plate chirowaveguide with $\xi_c = 0.001$ mho. Three regions are identified: fast-fast-wave region where $\beta < k_- < k_+$, fast-slow-wave region where $k_- < \beta < k_+$ and slow-slow-wave region where $k_- < k_+ < \beta$. It should be noted that there are pairs of bifurcated modes with common cut-off frequencies and differing propagation constants for any given frequency. One of the two curves of the bifurcated pairs corresponds to the odd mode whereas the other one corresponds to the even mode.

in a conventional waveguide filled with a nonchiral material. It should be noted that since chirowaveguides do not support TEM modes, the lowest cut-off frequency is not zero. From Fig. 4 we also see that the curves are bifurcated starting from the same cut-off frequency Ω_c and then split as $\beta a = k_+ a \cos\theta$ increases. In other words, for any given frequency greater than the lowest cut-off, there are pairs of modes with unequal propagation constants and common cut-off frequencies. This characteristic, which is one of the notable features of the parallel-plate chirowaveguide becomes apparent when we note that the dispersion relation given in (10) or (15) can be written as a product of two expressions. More explicitly we have

$$\Delta = \Delta_1 \cdot \Delta_2 = 0, \qquad (24)$$

where Δ is a shorthand for the dispersion relation given in (10), and Δ_1 and Δ_2 are found to be

$$\frac{\Delta_1}{2} = [\sqrt{1 - (\beta/k_+)^2} + \sqrt{1 - (\beta/k_-)^2}]$$

$$\cdot \sin\left(\frac{k_+ a\sqrt{1 - (\beta/k_+)^2} + k_- a\sqrt{1 - (\beta/k_-)^2}}{2}\right)$$

$$\pm [\sqrt{1 - (\beta/k_+)^2} - \sqrt{1 - (\beta/k_-)^2}]$$

$$\cdot \sin\left(\frac{k_+ a\sqrt{1 - (\beta/k_+)^2} - k_- a\sqrt{1 - (\beta/k_-)^2}}{2}\right).$$

$$(25)$$

It is clear from (24) that to have $\Delta = 0$, either Δ_1 or Δ_2 must be zero. This leads to a set of bifurcated modes originating from common cut-off frequencies. For each pair of bifurcated modes, the cut-off frequency can be obtained by having $\beta = 0$ in the dispersion relation (10), which results in $\Delta_1 = \Delta_2 = 0$. Then the expression for cut-off frequencies is obtained and already given in (22).

It is worth noting that although this and some other features of chirowaveguides appear to be similar with those of the gyrotropic (magnetized ferrite) waveguides [25], they are different in nature. Chirowaveguides, due to the reciprocal and isotropic nature of chiral materials, are reciprocal elements. Furthermore, in ferrite waveguides, some of the guided-wave characteristics change as the direction of the biasing magnetic field changes, whereas in chirowaveguides, the filling materials are isotropic, and there is no preferred direction. The dispersion curves in the fast-fast-wave region cross the line k_- at pairs of points which are designated as $B_1, C_1, B_2, C_2, \cdots$ in Fig. 4. Points $B_1, B_2, \cdots$ correspond to the curve $\Delta_1 = 0$, whereas points $C_1, C_2, \cdots$ belong to the curve $\Delta_2 = 0$. At these points, $\beta = k_- = k_+ \cos\theta_0$. The frequencies ω_{B_i} associated with points $B_1, B_2, \cdots$ are

$$\Omega_{B_i} \equiv \omega_{B_i} a \sqrt{\mu\epsilon} = \frac{\pi n}{\eta}\sqrt{\frac{\eta_c}{\xi_c}} \qquad (26)$$

with $n = 1, 2, 3, \cdots$, and frequencies ω_{c_i} (or Ω_{c_i}) associated with points $C_1, C_2 \cdots$ are the solutions to the following transcendental equation:

$$\tan\left(\Omega_{C_i}\frac{\eta}{\eta_c}\sqrt{\xi_c\eta_c}\right) = -\Omega_{C_i}\frac{\eta}{\eta_c}\sqrt{\xi_c\eta_c}\left(\frac{1 - \xi_c\eta_c}{1 + \xi_c\eta_c}\right).$$

$$(27)$$

It must be noted that for the nonchiral case where $\xi_c = 0$, the two lines k_+ and k_- become a single line k, the dispersion curves approach the line k asymptotically, points $B_1, B_2, \cdots$ join $C_1, C_2, \cdots$ and all together move to infinity and the frequencies associated with these points become infinitely large as expected from (26).

By applying the proper boundary conditions to (9a) and (9b), the coefficients A_{11}, A_{12}, A_{21}, and A_{22} are determined. These coefficients are related through the following expressions:

$$A_{11}\Delta_2 = A_{12}\Delta_1 \qquad (28a)$$

$$A_{21} = -\frac{S_1}{S_2}\frac{\cos(\sqrt{S_1}a/2)}{\cos(\sqrt{S_2}a/2)}A_{11} \qquad (28b)$$

$$A_{22} = -\frac{S_1}{S_2}\frac{\sin(\sqrt{S_1}a/2)}{\sin(\sqrt{S_2}a/2)}A_{12}. \qquad (28c)$$

Substituting these coefficients into (9a) and (9b) and using (7) and (5), we obtain the electric field components in the parallel-plate chirowaveguides. They are

$$E_x = -A_{11}\sqrt{\frac{S_1}{S_2}}\left\{k_+\sqrt{S_2}\sin(\sqrt{S_1}\,y)\right.$$

$$+ k_-\sqrt{S_1}\frac{\cos(\sqrt{S_1}a/2)}{\cos(\sqrt{S_2}a/2)}\sin(\sqrt{S_2}\,y)\right\}$$

$$+ A_{12}\sqrt{\frac{S_1}{S_2}}\left\{k_+\sqrt{S_2}\cos(\sqrt{S_1}\,y)\right.$$

$$\left. + k_-\sqrt{S_1}\frac{\sin(\sqrt{S_1}a/2)}{\sin(\sqrt{S_2}a/2)}\cos(\sqrt{S_2}\,y)\right\} \qquad (29a)$$

$$E_y = i\beta A_{11}\sqrt{\frac{S_1}{S_2}}\left\{ -\sqrt{S_2}\,\sin(\sqrt{S_1}\,y)\right.$$

$$+ \sqrt{S_1}\,\frac{\cos(\sqrt{S_1}a/2)}{\cos(\sqrt{S_2}a/2)}\,\sin(\sqrt{S_2}\,y)\right\}$$

$$+ i\beta A_{12}\sqrt{\frac{S_1}{S_2}}\left\{\sqrt{S_2}\,\cos(\sqrt{S_1}\,y)\right.$$

$$\left. - \sqrt{S_1}\,\frac{\sin(\sqrt{S_1}a/2)}{\sin(\sqrt{S_2}a/2)}\,\cos(\sqrt{S_2}\,y)\right\} \qquad (29b)$$

$$E_z = S_1 A_{11}\left\{\cos(\sqrt{S_1}\,y) - \frac{\cos(\sqrt{S_1}a/2)}{\cos(\sqrt{S_2}a/2)}\,\cos(\sqrt{S_2}\,y)\right\}$$

$$+ S_1 A_{12}\left\{\sin(\sqrt{S_1}\,y) - \frac{\sin(\sqrt{S_1}a/2)}{\sin(\sqrt{S_2}a/2)}\,\sin(\sqrt{S_2}\,y)\right\}.$$

$$\qquad (29c)$$

Similarly, the magnetic field components in the parallel-plate chirowaveguide can also be obtained.

There are several important features associated with (28) and (29). First, one must note that for any propagating mode inside a parallel-plate chirowaveguide, either $\Delta_1 = 0$ or $\Delta_2 = 0$. Each corresponds to an arm of the bifurcated modes in the dispersion diagram. Second, it follows from (28a) and the previous statement, that when Δ_1 equals zero, A_{11} vanishes, whereas when $\Delta_2 = 0$, A_{12} disappears. As a result, for that arm of the bifurcated mode corresponding to $\Delta_1 = 0$, E_z and H_z are odd functions of the y coordinate (with the origin of y axis located at the middle of the waveguide thickness) and E_x, E_y, H_x, and H_y are even functions of the y coordinate. This arm, therefore, corresponds to the even mode. On the other hand, for the other arm of the bifurcated mode corresponding to $\Delta_2 = 0$, E_z and H_z are even functions of y whereas E_x, E_y, H_z, and H_y are odd functions of the coordinate y. Hence, this arm corresponds to the odd mode. Finally it is worth noting that in the nonchiral limit when ξ_c approaches zero, one of the modes of the bifurcated pair approaches conventional TM mode, whereas the other approaches the usual TE mode in the parallel-plate waveguide.[2] As is well known, in parallel-plate waveguides filled with nonchiral isotropic materials, the dispersion curves for TE modes overlap those of the TM modes. Therefore, the two curves of bifurcated pairs in the parallel-plate chirowaveguides become a single curve as ξ_c approaches zero. Fig. 5 presents the electric field components inside a parallel-plate chirowaveguide as a function of y/λ for $\xi_c = 0.001$ mho and $a/\lambda = 0.56$.

The transverse components of the magnetic field $\mathbf{H}$ can be expressed in terms of the transverse components of $\mathbf{E}$ as follows:

$$\begin{bmatrix} H_x \\ H_y \end{bmatrix} = \begin{pmatrix} -i\xi_c & -\dfrac{\sqrt{k_+ k_-}}{\eta\beta} \\ \dfrac{\beta}{\eta\sqrt{k_+ k_-}} & i\xi_c \end{pmatrix}\begin{bmatrix} E_x \\ E_y \end{bmatrix} \qquad (30)$$

[2] When ξ_c approaches zero, $S_1 = S_2 = \sqrt{k^2 - \beta^2}$. From the dispersion relation given in (10), we get $\sin(\sqrt{k^2 - \beta^2}a) = 0$ resulting in $\sin(\sqrt{k^2 - \beta^2}a/2) = 0$ or $\cos(\sqrt{k^2 - \beta^2}a/2) = 0$. Therefore, care must be taken in finding the limits of $\sin(\sqrt{S_1}a/2)/\sin(\sqrt{S_2}a/2)$ and $\cos(\sqrt{S_1}a/2)/\cos(\sqrt{S_2}a/2)$ in (29) when ξ_c approaches zero.
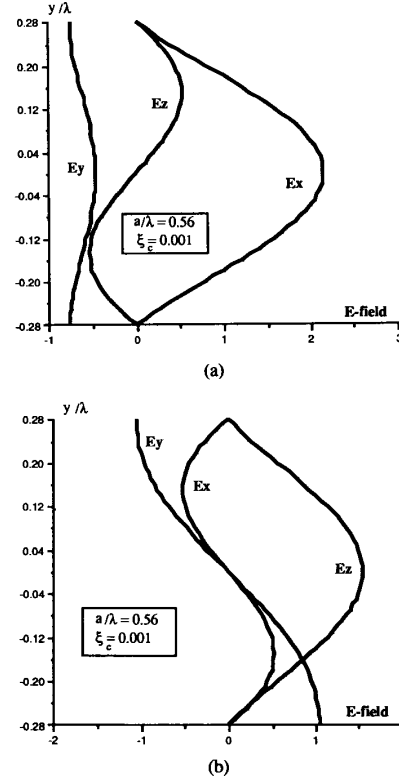

Fig. 5. Magnitudes of electric field components in a parallel-plate chirowaveguide as a function of y/λ for the fast-fast-wave region (Horizontal axis has an arbitrary unit). ξ_c and a/λ are taken to be 0.001 mho and 0.56, respectively. There are two bifurcated dispersion curves for each cut-off frequency. a) field profiles of the upper mode (even mode) of the first pair of bifurcated modes; and b) field profiles of the lower mode (odd mode) of the first bifurcated modes.

where $\eta = \sqrt{\mu/\epsilon}$. For $\xi_c = 0$, $k_+ = k_- = k$ and (30) reduces to the corresponding expression in a conventional parallel-plate waveguide.

2) Fast-Slow-Wave Region: In this region of the $\omega - \beta$ diagram, which is restricted to the region between the lines k_+ and k_-, i.e., $k_- < \beta < k_+$ for $\xi_c > 0$, θ is a real angle between $0°$ and θ_0, and φ is a pure imaginary angle $i\varphi_i$. In this region of the diagram, the dispersion relation is

$$2\sqrt{[1 - (\beta/k_+)^2][(\beta/k_-)^2 - 1]}$$

$$\cdot \{1 - \cos(k_+ a\sqrt{1 - (\beta/k_+)^2})\cosh(k_- a\sqrt{(\beta/k_-)^2 - 1})\}$$

$$+ \{2 - (\beta/k_+)^2 - (\beta/k_-)^2\}\,\sin(k_+ a\sqrt{1 - (\beta/k_+)^2})$$

$$\cdot \sinh(k_- a\sqrt{(\beta/k_-)^2 - 1}) = 0 \qquad (31)$$

and

$$k_+ \cos\theta = k_- \cosh\varphi_i = \beta. \qquad (32)$$

The dispersion curves in the fast-slow-wave region are presented in Fig. 4. In this region, the LCP plane waves propagate along the z-axis with a propagation constant greater than k_-. Therefore S_2 is imaginary and the LCP portion of the transverse field components are described by the hyperbolic
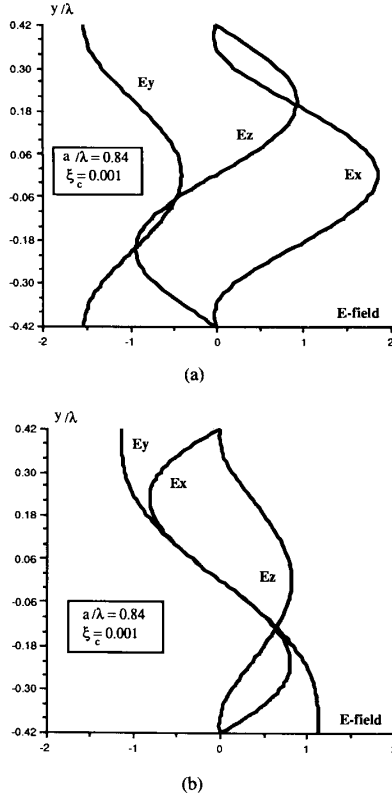
(a)

(b)

Fig. 6. Magnitudes of electric field components in a parallel-plate chirowaveguide as a function of y/λ for the fast-slow-wave region (Horizontal axis has an arbitrary unit). ξ_c and a/λ are taken to be 0.001 mho and 0.84, respectively. There are two bifurcated dispersion curves for each cut-off frequency. (a) field profiles of the upper mode (even mode) of the first pair of bifurcated modes. (b) Field profiles of the lower mode (odd mode) of the first bifurcated modes.

functions. Thus the LCP waves can be regarded as slow waves inside the waveguide. Such waves, in a simple parallel-plate waveguide filled with a nonchiral isotropic medium, could not satisfy the boundary conditions. In the parallel-plate chirowaveguide, however, since both RCP and LCP waves exist and the angle θ for RCP waves and S_1 are still real quantities, combination of these two sets of waves, RCP and LCP, gives rise to a physical solution satisfying the boundary conditions. This is another important feature of a chirowaveguide. In this region, the electric field components have the same form as in (29). However, S_2 is an imaginary quantity while S_1 is still real. Fig. 6 illustrates the variations of the electric field components as a function of y/λ for $a/\lambda = 0.84$ and $\xi_c = 0.001$ mho. Note that the field profiles in this figure are plotted for a value of a/λ different from that of Fig. 5. This is because, for a given pair of bifurcated modes, in order to be in the fast-slow-wave region of the dispersion diagram, the frequency must be greater than that of the fast-fast-wave region. Therefore, we choose the value of $a/\lambda = 0.84$, greater than that of Fig. 5 ($> a/\lambda = 0.56$ of Fig. 5) to stay on the same pair of bifurcated modes and to present the field profiles of the same pair in the fast-slow-wave region. If one desires to plot the field profiles in the fast-fast-wave and fast-slow-wave regions

for a single value of a/λ, the field profiles of two different pairs of bifurcated modes can be plotted.

The transverse components of the magnetic field $\mathbf{H}$ are related to the transverse components of $\mathbf{E}$ through the same relation given in (30).

3) Slow-Slow-Wave Region: The propagation constant β is greater than both k_+ and k_- in this region of $\omega - \beta$ diagram, which is between the β-axis and the line k_+. It turns out that in a parallel-plate chirowaveguide, a propagating mode does not exist in the slow-slow-wave region. This implies that, in a parallel-plate chirowaveguide, it is impossible to have a situation where both RCP and LCP component waves propagate as slow waves along the z-axis.

B. Evanescent Modes

For evanescent modes, the propagation constant must be a complex quantity. Let us take β to be $i\alpha$ where α is a real quantity. Thus $\gamma = -\alpha$ and both angles θ and φ are complex angles. That is

$$\theta = \theta_r + i\theta_i \tag{33}$$

$$\varphi = \varphi_r + i\varphi_i. \tag{34}$$

Since evanescent modes occur for frequencies below cut-off, the real part of the above angles, i.e., θ_r and φ_r must be 90°. Substituting $\beta = i\alpha$ into (10), and (33) and (34) into (12), we obtain

$$2\sqrt{[1 + (\alpha/k_+)^2][1 + (\alpha/k_-)^2]}$$
$$\cdot \{1 - \cos(k_+ a \sqrt{1 + (\alpha/k_+)^2}) \cos(k_- a \sqrt{1 + (\alpha/k_-)^2})\}$$
$$+ \{2 + (\alpha/k_+)^2 + (\alpha/k_-)^2\}$$
$$\cdot \sin(k_+ a \sqrt{1 + (\alpha/k_+)^2}) \sin(k_- a \sqrt{1 + (\alpha/k_-)^2}) = 0. \tag{35}$$

and

$$k_+ \sinh\theta_i = k_- \sinh\varphi_i = \alpha. \tag{36}$$

These equations are analyzed the same way the dispersion relations were treated for the propagating modes. The corresponding dispersion diagram is presented in Fig. 7. We note that the evanescent modes are also bifurcated. These double evanescent modes can be examined using a method similar to that used for propagating modes.

IV. CONCLUSION

We have studied and analyzed a new class of waveguides, *chirowaveguides*, which can be made of cylindrical waveguides containing homogeneous isotropic chiral materials. Propagation properties of electromagnetic waves guided by such waveguides have been investigated, and some of their novel and salient features have been discussed. It has been shown that due to coupling of Helmholtz equations for the longitudinal components of electric and magnetic fields, chirowaveguides are unable to support individual TE, TM or TEM modes. In these waveguides, modes are hybrid, TE and TM modes are always coupled and the coupling coefficients are proportional to the chirality admittance ξ_c of the material inside the wave-
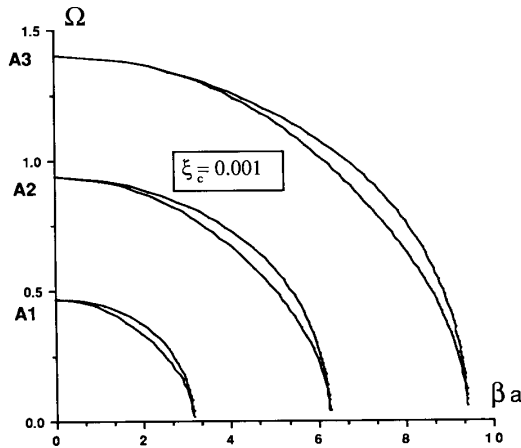
Fig. 7. Dispersion (Brillouin) diagram for evanescent modes in a parallel-plate chirowaveguide with $\xi_c = 0.001$ mho. It should be noted that there are pairs of bifurcated modes with common cut-off frequencies and differing attenuation constants for any given frequency. One of the two curves of the bifurcated pairs corresponds to the odd mode whereas the other one corresponds to the even mode.

guide. The rotation of the polarization ellipse of the electric field also occurs in chirowaveguides. However, this rotation differs from the phenomenon of Faraday rotation in longitudinally magnetized ferrite waveguides by the fact that the former is reciprocal and independent of the sense of wave propagation whereas the latter is not.

As an illustrative example, we have studied, in detail, a parallel-plate chirowaveguide and its properties. The dispersion relations, Brillouin diagrams, cut-off frequencies, propagating and evanescent modes for this chirowaveguide have been obtained and analyzed thoroughly. It has been shown that the propagating and evanescent modes are bifurcated. The three regions in the Brillouin diagram, viz. the fast-fast-wave, fast-slow-wave and slow-slow-wave regions have been identified. The additional region in the Brillouin diagram, i.e., the fast-slow-wave region is one of the important characteristics of chirowaveguides. For each region, the electromagnetic field components in the parallel-plate chirowaveguide have been analyzed.

Notable features of chirowaveguides can have potential applications in integrated optical devices, telecommunications electronic systems and printed-circuit elements. Optical chirowaveguides can be a new type of dielectric waveguides in integrated optics. The bifurcated modes which have common cut-off frequencies and unequal propagation constants for any given frequency can be used as multichannel networks in such optical components. The chirowaveguides can also be used in optical directional couplers. In directional couplers, which are also used as optical switches, the goal is to transfer energy from one fiber waveguide, say waveguide A into an adjacent fiber waveguide B. This energy transfer occurs through the overlapping of fields between the two waveguides. It is well known that the maximum energy transferred from guide A to guide B occurs when the phase-matched condition is fulfilled. That is when the wavenumbers of guide A and guide B are identical. Since chirowaveguides exhibit mode bifurcation,

even for a single-mode design, at any frequency of operation, one can have two modes with two different guide wavenumbers propagating down the chirowaveguide A. In this case, it would be sufficient, for a optimum energy transfer from guide A to guide B, to have only one of these two wavenumbers matched with the wavenumbers of the neighboring waveguide B. This would offer a great flexibility and reliability in the design of optical directional couplers and photonic switches.

Due to the fact that the parallel-plate chirowaveguides, unlike their nonchiral counterparts, cannot support modes with zero cut-off frequency, they can be used as substrates and/or superstrates in integrated-circuit antennas to reduce significantly the surface-wave power, and consequently increase the radiation efficiency of such antennas.

REFERENCES

[1] N. Engheta and P. Pelet, "Modes in chirowaveguides," Opt. Lett., vol. 14, no. 11, pp. 593-595, 1989.
[2] N. Engheta and D. L. Jaggard, "Electromagnetic chirality and its applications," IEEE Antennas Propagat. Soc. Newsletter, vol. 30, no. 5, pp. 6-12, 1988.
[3] D. F. Arago, "Sur une modification remarquable qu'éprouvent les rayons lumineux dans leur passage à travers certains corps diaphanes, et sur quelques autres nouveaux phénomènes d'optique," Mém. Inst., vol. 1, pp. 93-134, 1811.
[4] J. B. Biot, "Mémoire sur un nouveau genre d'oscillations que les molecules de la lumière éprouvent, en traversant certains cristaux," Mém. Inst., vol. 1, p. 1, 1812.
[5] ——, "Sur les rotations que certaines substances impriment aux axes de polarisation des rayons lumineux," Mém. Acad. Sci., vol. 2, p. 41, 1838.
[6] ——, "Mémoire sur la polarisation circulaire et sur ses applications à la chimie organique," Mém. Acad. Sci. 13, p. 93, 1838.
[7] L. Pasteur, "Sur les relations qui peuvent exister entre la forme cristalline, la composition chimique et le sens de la polarisation rotatoire," Ann. Chim. Phys., vol. 24, pp. 442-459, 1848.
[8] F. M. Jaeger, Lectures on the Principle of Symmetry. London: Cambridge Univ. Press, 1917.
[9] H. Weyl, Symmetry. Princeton, NJ: Princeton Univ. Press, 1952.
[10] D. L. Jaggard, A. R. Mickelson, and C. H. Papas, "On electromagnetic waves in chiral media," Appl. Phys., vol. 18, pp. 211-216, 1979.
[11] J. A. Kong, Theory of Electromagnetic Waves. New York: Wiley, 1975.
[12] E. J. Post, Formal Structure of Electromagnetics. Amsterdam: North-Holland, 1962.
[13] K. F. Lindman, Ann. Phys., vol. 63, p. 621, 1920.
[14] ——, Ann. Phys., vol. 69, p. 270, 1922.
[15] W. H. Pickering, experiment performed at Caltech, 1945, private communication.
[16] N. Engheta and A. R. Mickelson, "Transition radiation caused by a chiral plate," IEEE Trans. Antennas Propagat., vol. AP-30, pp. 1213-1216, 1982.
[17] S. Bassiri, C. H. Papas, and N. Engheta, "Electromagnetic wave propagation through dielectric-chiral interface and through a chiral slab," J. Opt. Soc. Am., vol. A5, no. 9, pp. 1450-1459, 1988.
[18] J. A. Kong, "Theorems of bianisotropic media," Proc. IEEE, vol. 60, pp. 1036-1046, 1972.
[19] M. P. Silverman, "Reflection and refraction at the surface of a chiral medium: Comparison of gyrotropic constitutive relations invariant or noninvariant under duality transformation," J. Opt. Soc. Am.,vol. A3, pp. 830-837, 1986.
[20] A. Lakhtakia, V. K. Varadan, and V. V. Varadan, "Scattering and absorption characteristics of lossy dielectric, chiral, nonspherical objects," Appl. Opt., vol. 24, pp. 4146-4154, 1985.
[21] S. Bassiri, N. Engheta, and C. H. Papas, "Dyadic Green's function and dipole radiation in chiral media," Alt. Freq., vol. LV-2, pp. 83-88, 1986.
[22] N. Engheta and S. Basiri, "One- and two-dimensional dyadic Green's function in chiral media," IEEE Trans. Antennas Propagat., vol. 37, no. 4, pp. 512-515, Apr. 1989.
[23] D. L. Jaggard,, X. Sun, and N. Engheta, "Canonical sources and

duality in chiral media," *IEEE Trans. Antennas Propagat.*, vol. 36, no. 7, pp. 1007–1013, July 1988.

[24] M. L. Kales, "Modes in wave guides containing ferrites," *J. Appl. Phys.*, vol. 24, no. 5, pp. 604–608, 1953.

[25] A. Van Trier, "Guided electromagnetic waves in anisotropic media," *Appl. Sci. Res.*, vol. B3, pp. 305–371, 1953.

[26] H. Gamo, "The Faraday rotation of waves in a circular waveguide," *J. Phys. Soc. Japan*, vol. 8, no. 2, pp. 176–182, 1953.

[27] R. E. Collin, *Field Theory of Guided Waves*.   New York: McGraw-Hill, 1960.

[28] P. Hlawiczka, *Gyrotropic Waveguides*. New York: Academic, 1981.

Philippe Pelet (S'88), for a photograph and biography please see page 1452 of the November 1989 issue of this TRANSACTIONS.

Nader Engheta (S'80–M'82–SM'89), for a photograph and biography please see page 330 of the March 1988 issue of this TRANSACTIONS.